Journal of Asian Earth Sciences 290 (2025) 106661

Contents lists available at ScienceDirect

Journal of Asian Earth Sciences

journal homepage: www.elsevier.com/locate/jseaes

Updating the timeline of faunal endemism in Balkanatolia, the biogeographic province connecting Europe, Asia and Africa

Leny Montheil [a,*], Alexis Licht [a], Deniz İbilioğlu [b], Paul Botté [a], Faruk Ocakoğlu [c], François Demory [a], Gilles Ruffet [d], Abel Guihou [a], Mustafa Kaya [e], Benjamin Raynaud [f], Mehmet Serkan Akkiraz [b], Pierre Deschamps [a], Grégoire Métais [f], Pauline Coster [g], K. Christopher Beard [h,i]

[a] Aix Marseille University, CNRS, IRD, INRAE, CEREGE, Aix-en-Provence, France
[b] Department of Geological Engineering, Kütahya Dumlupınar University, Kütahya, Turkey
[c] Department of Geological Engineering, Eskişehir Osmangazi University, Eskişehir, Turkey
[d] CNRS (CNRS/INSU), UMR 6118 Géosciences Rennes, Université de Rennes, Rennes, France
[e] Department of Geological Engineering, Middle East Technical University, Ankara, Turkey
[f] Centre de recherches en Paléontologie - Paris (CR2P), Muséum National d'Histoire Naturelle, CNRS, Paris, France
[g] Réserve naturelle nationale géologique du Luberon, Unesco Global Geopark, Parc naturel régional du Luberon, Apt, France
[h] Biodiversity Institute, University of Kansas, Lawrence, KS, USA
[i] Department of Ecology and Evolutionary Biology, University of Kansas, Lawrence, KS, USA

ARTICLE INFO

Keywords:
Biogeography
Endemism
Dating
Balkanatolia
Terrestrial Fauna Dispersal

ABSTRACT

Balkanatolia is a Paleogene insular biogeographic province, spanning from southeastern Europe to the Caucasus. It is located at the crossroads of Asia, Europe, and Africa, from which it remained isolated until the late Eocene, fostering endemism, particularly among mammals. However, the timing of emergence of Balkanatolia as an independent biogeographic province remain debated due to the paucity of the fossil record and loose age constraints. Here, we refine this timing by combining magnetostratigraphy, biostratigraphy, geochronology and sedimentology to date three fossil sites of central Anatolia (Çamili Mezra, Çiçekdagi, and Bultu-Zile). These sites have yielded remains of embrithopods, a clade of large herbivorous afrotherian mammals that originated in Africa and dispersed across the Neotethys to reach Balkanatolia where they diversified. The Çamili Mezra locality yield an age spanning from 46.2 Ma to 43.5 Ma, likely around ~ 45 Ma based on accumulation rates, the Çiçekdagi locality is dated to the very base of Chron C20r (ca. 46.2 Ma) and the Bultu-Zile locality yield overlapping 46.5 ± 1.0 Ma and 45.1 ± 0.9 Ma ages. Overall, these fossil localities are coherently dated to the early Lutetian and represent the oldest unequivocally embrithopod-bearing sites of the northern Neotethysian shores. They provide an early Lutetian minimum age for Balkanatolian endemism, its emergence as an independent biogeographic province and for the overwater dispersal of embrithopods out of Africa.

1. Introduction

Island archipelagos represent one third of Earth's biodiversity hotspots (Myers et al., 2000). Island environments promote distinctive evolutionary trajectories, especially among mammals and other vertebrates, that contrast with those on continental environments, resulting in demonstrable anatomical, physiological and behavioral differences (MacArthur and Wilson, 1963). The study of insular Plio-Pleistocene faunas has significantly helped in describing and understanding these differences (van der Geer et al., 2011) and has highlighted multiple phenomena including the potential causes of extinctions (Steadman et al., 2005), anachronistic range extensions (Vartanyan et al., 1993), and common island syndromes such as dwarfism and gigantism (Köhler and Moyà-Solà, 2004). However exhaustive, they have contributed little to our knowledge of how island faunas are assembled over the longer time scale of macroevolutionary processes (several Ma), nor have they provided a basis for evaluating models of island biogeography (MacArthur and Wilson, 1963, 1967).

* Corresponding author.
E-mail address: montheil@cerege.fr (L. Montheil).

https://doi.org/10.1016/j.jseaes.2025.106661
Received 3 December 2024; Received in revised form 28 April 2025; Accepted 15 May 2025
Available online 15 May 2025

During the Paleogene, parts of Eastern Europe and the Middle East were an archipelago of islands designated as Balkanatolia (Licht et al., 2022). The areal extent and connectivity of this biogeographic province fluctuated with tectonic changes induced by the closure of the Neotethys Ocean and with global eustatic variations (Fig. 1). During the Paleocene and most of the Eocene, this mosaic of terranes remained separated from other landmasses by seaways of variable breadth. This isolation remained significant until the latest Eocene, when regional uplift and a major marine regression increased the terrestrial connectivity of Balkanatolia with Asia, then with Europe and Africa (Barrier et al., 2018; Métais et al., 2023). Balkanatolia is at the crossroads of major biogeographic realms (i.e. Asia, Europe and Africa) and its specific paleogeographic setting and evolution recalls modern Wallacea (the archipelago between Sundaland, Sulawesi, and the Australia-Papua shelf). This makes the area unique for studying island biotas over macroevolutionary timespans (Beard et al., 2021).

The Eocene fauna of Balkanatolia comprised a distinctive assemblage of endemic mammals including afrotherian embrithopods that are large herbivorous mammals potentially exhibiting a semi-aquatic lifestyle, and smaller metatherians (Maas et al., 1998; Métais et al., 2018, 2024; Beard et al., 2023). These taxa are of Gondwanan origin and most likely dispersed from Africa sometime during the Paleogene (Métais et al., 2018; Beard et al., 2023). It also includes anachronistic survivors of an otherwise Paleocene European pleuraspidotheriid clade (Métais et al., 2016), with only bats (Jones et al., 2019) and primates (Beard et al., 2021) showing biogeographic affinities with Asia. The end of Balkanatolian endemism is relatively well-constrained as late middle Eocene, when Asian ungulates colonized Balkanatolia in the late Bartonian (ca. 40–38 Ma), following the establishment of a continuous terrestrial corridor across the central segment of the Neotethyan margin (Licht et al., 2022). However, when Balkanatolia emerged as an independent mammalian biogeographic province remains unknown because of the lack of well-dated early Paleogene mammalian-bearing fossil locality.

Documenting the onset and duration of endemism is critical to evaluate the assembly and diversification mechanisms of the unique Balkanatolian fauna. The presence of pleuraspidotheriids in Balkanatolia during the late Lutetian (which went extinct at the end of Paleocene elsewhere) indicate that endemism must have been a long-standing feature persisting for millions of years in the Eocene, despite the proximity of multiple continental biogeographic provinces (Métais et al., 2018) (Table 1). Moreover, the striking absence of rodents, perissodactyls, artiodactyls, carnivorans, and other clades that became ubiquitous across Laurasia during the earliest Eocene suggests a period of isolation starting at least during the latest Paleocene (Licht et al., 2017; Métais et al., 2018). The oldest sites yielding embrithopod taxa, Eski Celtek (Métais et al., 2012) and Çamili Mezra (Métais et al., 2024) are qualitatively attributed to the early Eocene based on biostratigraphic constraints of nearby marine units (Table 1). Nonetheless, the chronology of Balkanatolian endemism remains elusive because few sites yielding endemic taxa have been precisely dated (Licht et al., 2022).

This study documents the age of multiple, previously-published paleontological sites of central Anatolia yielding iconic endemic taxa from Balkanatolia. We combine magnetostratigraphic, biostratigraphic, geochronological and sedimentary approaches to date the paleontological sites and better constrain the age of Balkanatolian endemism, as well as the evolutionary history of embrithopods, a key Balkanatolian clade.

2. Geological context

Balkanatolia was defined by Licht et al. (2022) as a semi-continuous strip of land during the Paleocene and Eocene, located between the western European craton and the Cimmerian terranes of the Middle East

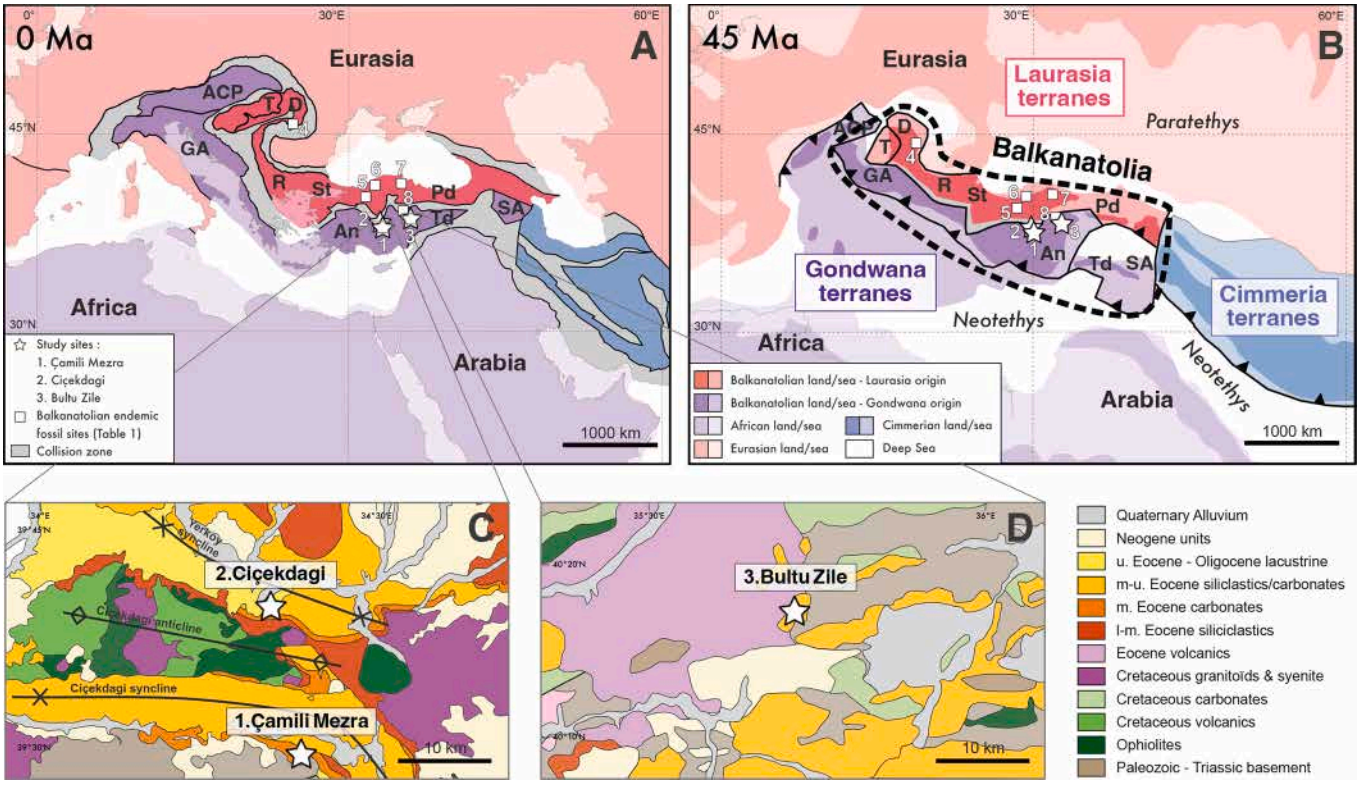

Fig. 1. (A) Present-day structural map of the Balakanatolian tectonic terranes. ACP: Alcapa, An-TD: Anatolide-Tauride, D: Dacia, GA: Greater Adria, Pd: Pontides, R: Rhodope, SA South Armenia, St: Standja Massif, T: Tisza. (B) Middle Eocene structural map of Balakanatolia displaying localities yielding endemic Balkanatolian taxa. Stars: sites of study with 1: Çamili Mezra; 2: Ciçekdagi and 3: Bultu-Zile. Dots: other fossil sites with 4: Hateg; 5: Orhaniye; 6: Boyabat; 7: Eski Celtek and 8: Bogazliyan. (C) Simplified geological map of the Ciçekdagi and Çamili Mezra area. (A), (B) and (C) maps are modified from Licht et al., 2022. (D) Simplified geological map of the Bultu-Zile area, modified from Uguz et al. (2002).

Table 1
Synthesis of endemic Balkanatolian fossil sites.

Location #	Locality name	Terrane	Chronostratigraphic Age	Geochronological Age	Age constraints	Fossil land mammals	References
1	Southern Cankiri Basin (Camili Mezra mine; Turkey)	Taurides	late Ypresian – Lutetian	51.1–41 Ma	Unit yielding Lutetian pollen assemblages and below late late Ypresian to Lutetian limestones.	Embrithopoda (*Palaeoamasia kansui*)	Nairn et al., 2013; Akgün et al., 2002; Gülyüz et al., 2013
2	Southern Cankiri Basin (Cicekgadgi mine; Turkey)	Taurides	Lutetian	48.6–41 Ma	Unit above Ypresian basalts and below uppermost Lutetian limestones, yield middle Eocene pollen assemblages.	Embrithopoda (*Palaeoamasia kansui, Crivadiatherium sahini, Crivadiatherium sevketseni*)	Akgün et al., 2002; Schweitzer et al., 2007; Erdal et al., 2016; Métais et al., 2024
3	Southern Cankiri Basin (Yozgat area, Bultu-Zile; Turkey)	Taurides	Lutetian	48.6–41 Ma	Unit yielding middle to upper Eocene pollen assemblages and is below Lutetian limestones.	Embrithopoda (*Palaeoamasia kansui*)	Kaya, 1995; Akkiraz et al., 2008
4	Hateg Depression (Roumania)	Dacia-Tisza	Middle to upper Lutetian	46–43 Ma	Unit correlated to nearby deposits attributed to Biozone NP15.	Embrithopoda (*Crivadioatherium Mackennai, C. Iliescui*)	Radulesco and Samson, 1987; Proust and Hosu, 1996
5	Orhaniye Basin (Turkey)	Pontides	Upper Lutetian	44–43 Ma	Age constrained by detrital zircon ages and magnetostratigraphy.	Embrithopoda (*Palaeoamasia* sp.) Pleuraspidotheriidae (*Hilalia saribeya, H. robusta, H. sezerorum, H. Selanneae*), Marsupiala (*Anatoliadelphys maasae, Galatiadelphys minor, Orhaniyeia nauta*), Primate (*Nesomomys bunodens*), Palaeochinopterygidae bat (*Anatolianycteris insularis*)	Licht et al., 2017; Métais et al., 2018; Jones et al., 2019
6	Boyabat Basin (Turkey)	Pontides	Lutetian	48.6–41 Ma	Unit unconformably overlying upper Maastrichtian deposits and below uppermost Lutetian limestones, correlated to nearby Lutetian units.	Embrithopoda (*Palaeoamasia kansui, Axainamasia sandersi*)	Ozansoy, 1966; Sen and Heintz, 1979; Métais et al., 2024
7	Suluova Basin (Eski-Celtek Mine; Turkey)	Pontides	Paleocene to Ypresian	56–48.6 Ma	Unit unconformably overlying upper Maastrichtian deposits and below lower Lutetian limestones, correlated to nearby Lutetian units.	Embrithopoda (*Palaeoamasia kansui*), Pleuraspidotheriidae (*Parabunodon anatolicum*)	Métais et al., 2012; Erdal et al., 2016
8	Bogazlıyan-YeniFakili (Turkey)	Taurides	Ypresian – Lutetian	56–41 Ma	Unit unconformably overlying upper Maastrichtian deposits and below Lutetian limestones, correlated to nearby Ypresian to Lutetian units.	Embrithopoda (*Palaeoamasia kansui*)	Ozansoy, 1966; Sen and Heintz, 1979

(Fig. 1A). In the north, the basement of Balkanatolia comprises Laurasia-derived terranes (Tisza, Dacia, Rhodope and Standja Massif and Pontides) that were separated from Laurasia by back-arc spreading during the Mesozoic (van Hinsbergen et al., 2020). To the south, the basement of Balkanatolia comprises individual terranes that rifted from Gondwana (Alcapa, Greater Adria, Anatolide-Taurides and South Armenia) and accreted onto the Laurasia-derived terranes during the late Cretaceous-early Paleogene (Mueller et al., 2022). This accretion was a long and protracted process that started in the Albian in western Balkanatolia (Dacia-Tisza accretion) and concluded in the late middle Eocene in eastern Balkanatolia with the collision between the eastern Pontides and the Taurides (van Hinsbergen et al., 2020).

During the Paleocene and most of the Eocene, this mosaic of terranes remained permanently separated from other landmasses by relatively narrow seaways (Fig. 1B): (1) from Africa by the western branch of the Neotethys (ca 200–400 km wide); (2) from the Western European Craton and Eurasia by the Paratethys (100 km wide in the Swiss Foreland Basin, to 500 km wide in the Black Sea); (3) from Middle Eastern Cimmerian terranes by remnant seaways connecting the Neotethys to the Paratethys on both sides of the Lesser Caucasus (less than 100 km wide) (Poblete et al., 2021) (Fig. 1B). Balkanatolia experienced numerous local episodes of partial inundation and emersion during the Paleogene (Barrier et al., 2018) and was fragmented into multiple islands during most of the Paleocene and early Eocene (Alpine, Balkanian, Tisza and Dinarian Highs, Anatolian and Pontian lands of Popov et al. (2004)). Many of the shallow seaways separating Balkanatolian islands retreated during the Lutetian, increasing land connectivity and paving the way to its connection with Asia in the late Bartonian (Barrier et al., 2018).

Our knowledge of the endemic Balkanatolian fauna comes from eight Ypresian to Lutetian fossil localities (Fig. 1) (Table 1). With the exception of the Hateg Depression in Romania (site 4 in Fig. 1) (Akkiraz et al., 2008), all these localities are found in Anatolia. Seven of these localities are compiled in Licht et al. (2022), and an eighth locality, Çamili Mezra, was more recently published (Métais et al., 2024). Two of these localities have relatively "tight" age constraints: (1) the Hateg Depression locality in Romania is attributed to biozone NP15 based on nearby marine units, providing a middle Lutetian age (46–43 Ma) (Radulesco and Samson, 1987); (2) the Uzunçarşıdere Formation (UCF) fauna from central

Anatolia, in the Orhaniye Basin, is dated to the late Lutetian (44–43 Ma) by a combination of magnetostratigraphy and U-Pb dating of detrital zircons (Licht et al., 2017). All the other sites are either attributed to the Ypresian or the Lutetian, or both, based on regional correlations of underlying or overlying marine units (Barrier et al., 2018). This study focuses on three of these poorly dated fossil localities: Çamili Mezra, Çiçekdagi and Bultu-Zile (Fig. 1B).

Çamili Mezra has yielded material of two embrithopod species, *Crivadiatherium sevketseni* and *C. sahini* (Métais et al., 2024). The locality is located at the southern edge of the Cankiri Basin, in the Çiçekdagi syncline (N39°29′05.2″ E34°22′14.8″; Fig. 1C). The fossil horizon is a coal seam of 1 to 5 m at the top of the Barakle Formation, which is the oldest Paleogene unit in the area. The continental Barakle Formation unconformably overlain the crystalline basement. It consists of 5 to 300 m of greenish to brown sandstones and laminated mudstones, of poorly cemented conglomerates, and of lignite seams in its uppermost beds (Fig. 2). Pollen from these lignites suggests a Lutetian age for the top of the Barakle Formation (Akgün et al., 2002). It grades into the Cevirme Formation, a marine, marl-dominated unit with rare tabular sandstone and limestone beds. This uppermost part of the Cevirme Formation is transitional with the overlying Kocaçay Limestone, which is composed of ~ 100 m of massive limestones alternating with thin marl beds (Fig. 2). In the Cankiri Basin, the Kocaçay Limestone is attributed to the Lutetian (Nairn et al., 2013). In the Çiçekdagi syncline, this unit yet revealed a benthic foraminiferal assemblage correlated to the late Ypresian SB-11–12 Zones (ca. 51.0 to 48.0 Ma) (Schweitzer et al., 2007).

The Çiçekdagi coal mine yielded remains of the embrithopod *Palaeoamasia kansui* (Erdal et al., 2016). The Cicekgdadi coal mine is located ca. 10 km to the north of Çamili Mezra, basinward within the Cankiri Basin, in the Yerkoy syncline (N39°34′47.4″ E34°25′13.8″; Fig. 1C). The lignite layer is now poorly exposed following the drowning of the open pit. Like in Çamili Mezra, the lignite bed reflects the continental-to-marine transition of an Eocene marine transgression. It is stratigraphically located at the top of the Barakle Formation, which grades into the overlying marine marls, which are grouped here under the Bogazkoy Formation (Fig. 2). Pollen from the mine suggests a Lutetian age for the fossil bed (Akgün, 2002). The Bogazkoy Formation includes a volcanic member, the Alimpinar volcanics, made of basalts and mafic volcanic conglomerates. ^{40}Ar-^{39}Ar dating of one of these basalts does not yield a stable plateau age but is coherent with a Lutetian age (Gülyüz et al., 2013). Limestones attributed to the Kocaçay Formation overlay the Alimpinar volcanics.

Bultu-Zile yielded complete jaws of the embrithopod *Palaeoamasia kansui* (Kaya, 1995). The area lies on the southern edge of the Pontides Terrane, and its Paleogene stratigraphic sequence follows the overall same succession as the nearby Cankiri Basin (Akgün et al., 2002). The fossil horizon is a 20- to 60-meter-thick coal seam within the Beynamaz volcanic member of the Eocene Meryemdere Formation (Fig. 2). The Meryemdere Formation consists of marine marls and sandstones that yielded Lutetian to Priabonian nannoplankton and foraminifera (Sevin

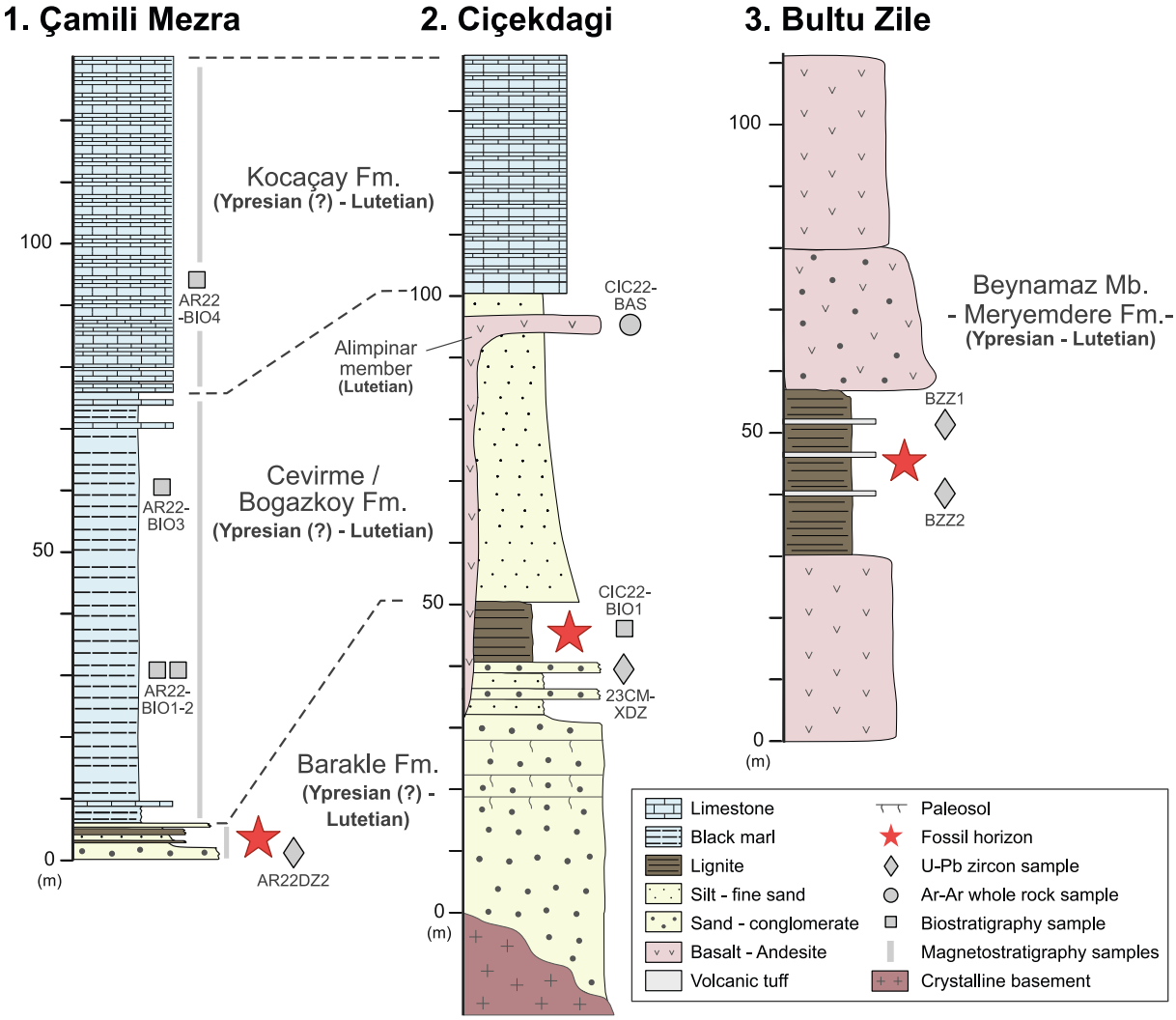

Fig. 2. Simplified stratigraphy and age constraints of Çamili Mezra, Çiçekdagi and Bultu-Zile sections.

et al., 2014). The Beynamaz Member is 300-meter-thick and comprises andesites, tuffs and volcanic conglomerates and unpublished radiometric ages suggest an Ypresian to Lutetian age (Sevin et al., 2014) (Fig. 2). The coal seam that yields vertebrate remains is mined in two localities close to Emirkoyu village; both of them yield fossil vertebrate material. It is poorly exposed in the first mine (site BZ1, 40°19′16.7″N, 35°41′48.4″E) where the pit has been flooded. In the second mine (site BZ2, 40°18′30.4″N, 35°40′40.3″E), lignite beds alternate with rare organic-rich mudstones, tuff and tuffaceous sandstones.

3. Methods

The dating method was selected based on the lithology available at each site (Fig. 2). At Çamili Mezra, fine-grained sediments (i.e., siltstones, black marls, and limestones) were collected for magnetostratigraphy, black marls for biostratigraphy, and a sandstone for U-Pb zircon dating. At Ciçekdagi, a lignite bed was sampled for biostratigraphy, along with a sandstone for U-Pb zircon dating and a basalt for ^{40}Ar-^{39}Ar dating. At Bultu-Zile, two volcanic tuffs were sampled for U-Pb zircon dating (Fig. 2).

3.1. Magnetostratigraphy

In Çamili Mezra, we logged and sampled a 130-meter-thick sedimentary section across the Barakle Formation (including the fossil horizon), the Cevirme and Kocaçay Formations (Fig. 2). Rock samples for magnetostratigraphic dating were collected from a segmented and rotated mine prospecting vertical borecore that obliquely crosscut the regional bedding (N305, 40°NNE). A total of 108 rock samples were extracted perpendicularly to the vertical mining borecore using a portable electric drill (SI Fig. 1), resulting in a horizontal dip and an unconstrained azimuth as the borecore is segmented and do not exhibit consistent bedding. To re-orient our sample in geographic and tectonic coordinates, we use the apparent bedding of each sample constrained by the magnetic foliation estimated from Anisotropy of the Magnetic Susceptibility analysis (SI Data 2, SI Table 2).

Collected samples consist of siltstones in the Barakle formation, of black marls in the Cevirme formation, and of black marls and limestone in the Kocaçay formation. Remanent magnetizations were investigated by alternating field (AF) stepwise demagnetization with field increments of 5 mT from 0 to 40 mT and of 10 mT from 40 to 100 mT and by thermal (TH) demagnetization with temperatures increments of 20 °C, 30 °C, 40 °C or 50 °C from room temperature up to 660 °C, using the Superconducting Rock Magnetometer SRM760R (2G enterprises) of CEREGE (Aix-Marseille University). AF demagnetization was preferred to thermal demagnetization to avoid medium temperature (300–400 °C) mineralogic changes of marls. ChRM directions were interpreted by means of the principal component analysis (Kirschvink, 1980). Demagnetization data were plotted in Zijderveld diagrams (Zijderveld, 1967) and stereographic projection with PuffinPlot software package (Lurcock and Wilson, 2012). Detailed results are available in Supplementary Information 1. Samples that were unstable during demagnetization are defined as unreliable samples and not considered in our interpretations. ChRMs data were grouped in magnetozones based on polarity (normal or reverse) and compared with the Geomagnetic Polarity Timescale 2020 (Speijer et al., 2020).

3.2. Biostratigraphy

Four samples in Çamili Mezra and one sample from the Ciçekdagi mine were selected for ostracod and foraminifera biostratigraphic dating. In Çamili Mezra, they comprise two samples from the base of the Cevirme Formation (AR22-BiO1 and −BiO2), one sample from the middle of the Cevirme Formation (AR22-BiO3), and one sample from the base of the Kocaçay Formation (AR22-BiO4). In Ciçekdagi, where the fossil bed is nowadays flooded and inaccessible, we sampled mine tailing material yielding lignite and tooth enamel fragments (sample CIC22-BiO1). Micropaleontological identification was carried out at Kütahya Dumlupınar University, Türkiye; detailed results and microphotographs are available in Supplementary Information 2.

3.3. U-Pb dating

Four rock samples were selected for U-Pb dating of detrital/volcanic zircons. These include: one sandstone in the Barakle Formation in Çamili Mezra, directly below the fossil bed (sample AR22DZ2), one sandstone from Barakle Formation in the Ciçekdagi mine, between 5 and 10 m below the supposed location of the lignite bed (sample 23CMXDZ) and two volcanic tuffs, one in each of the Bultu-Zile mines, found within the lignite (sample BZZ1 at mine BZ1 & sample BZZ2 at mine BZ2). Zircon crystals were separated by standard heavy liquid techniques and mounted in epoxy resin. U-Pb ages were generated using laser-ablation inductively-coupled-plasma mass-spectrometry (LA-ICPMS) at the Envitop analytical facility at CEREGE (Centre for Research and Education in Environmental Geosciences), with an Element XR ICP-MS connected to an ESI laser ablation system (NWR 193 nm). Detailed methods for extraction, analysis, and data reduction can be found in Licht et al. (2024). Maximum depositional age for detrital samples and crystallization age for volcanic samples were calculated with ^{206}Pb/^{238}U dates using TuffZirc (Ludwig, 2003) on concordant grains only. The final age uncertainty around crystallization ages is the quadratic sum of the uncertainty of TuffZirc age calculation and of the systematic uncertainty (1.31 % 2 *s* for the 238U/206Pb ratios). We calculated the maximum depositional age for each detrital sample as the weighted average of the youngest concordant zircon dates when the youngest three or more dates overlap (Dickinson and Gehrels, 2009). Detailed U-Pb data are given in Supplementary Information 3.

3.4. ^{40}Ar-^{39}Ar dating

One basalt sample (CIC22-BAS) from a dyke of the Alimpinar volcanics in the Ciçekgdagi mine was taken for ^{40}Ar-^{39}Ar dating. The dyke cross-cut the lignite mine and is thus younger than the fossil site (Fig. 2). A millimeter-sized whole rock single grain (CIC22-BAS) was analyzed by step-heating using a CO_2 laser probe coupled to a MAP 215 mass spectrometer. The procedure was described by Ruffet et al. (1991, 1995, 1997). Sample CIC22-BAS was irradiated in the 8E facility of the MacMaster Nuclear Reactor (Hamilton, Ontario, Canada). Irradiation lasted 175.633 h with a global efficiency (J/h) of 6.57 x $10^{-5}h^{-1}$. The irradiation standard was amphibole Hb3gr (Turner et al., 1971; Roddick, 1983; Jourdan et al., 2006; Renne et al., 2010) – 1081.0 ± 1.2 Ma according to Renne et al. 2010, Renne et al., 2011. Blanks were routinely performed on each first or third/fourth run, and are subtracted from the subsequent sample gas fractions. Apparent age errors are reported at the 1σ level and do not include errors in the $^{40}Ar^*/^{39}Ar_K$ ratio, monitor age and decay constant. Usually, we consider that a plateau age can be calculated when 70 % or more of the $^{39}Ar_K$ is released in at least three or more contiguous steps defining apparent ages that agree with the integrated age of the plateau segment to within 2σ. In the present case, only a pseudo-plateau age (similar concordance criteria) (Cheilletz et al., 1999) could be calculated for sample CIC22-BAS because the plateau segment contained less than 70 % of the released $^{39}Ar_K$. The errors in the $^{40}Ar^*/^{39}Ar_K$ ratio and age of the monitor and decay constant are included in the final calculation of the error margins of the plateau ages. $^{40}Ar/^{39}Ar$ ages are reported with 1σ errors. Analytical data and parameters used for calculations (e.g. isotopic ratios measured on pure K and Ca salts; mass discrimination; atmospheric argon ratios; J parameter; decay constants) and reference sources are available in Supplementary Information 3.

4. Results

4.1. Magnetostratigraphy of Çamili Mezra

Intensities of the Natural Remanent Magnetization ranges from 0.03 to 10.1 mA/m for the limestone specimens, from 0.1 to 95.6 mA/m for the black marl specimens and from 0.1 to 1.7 mA/m for the siltstone specimens (Supplementary Information 1). In alternating field (AF) stepwise demagnetizations, the limestones and the black marls demagnetization diagrams usually show a consistent to noisy decay toward the origin (Fig. 3A, 2B, 2C, 2D). The siltstones display noisier diagrams, potentially due to the presence of multi-domain grains (Fig. 3E, 2F). Most samples show a consistent component with medium unblocking coercivities (10–20 mT to 60–80 mT). This component is interpreted as the Characteristic Remanent Magnetization (ChRM). For some samples, a second, low stability component is recognized for low coercivity increments and interpreted as a present-day field overprint (Fig. 3D). Thermal (TH) stepwise demagnetization usually shows a consistent to noisy decay toward the origin (Fig. 3G). The samples display a single component with medium unblocking temperature (300 °C to 600 °C), interpreted as the ChRM. In the black marl samples, an abrupt increase of the intensity and inconsistent directions is observed above 300 °C increments (Fig. 3H) interpreted as a mineralogical change during heating. A positive match of the Common True Direction indicate that the ChRM directions are distributed in two antipodal groups (SI Fig. 2). The presence of antipodal reverse and normal polarities together with

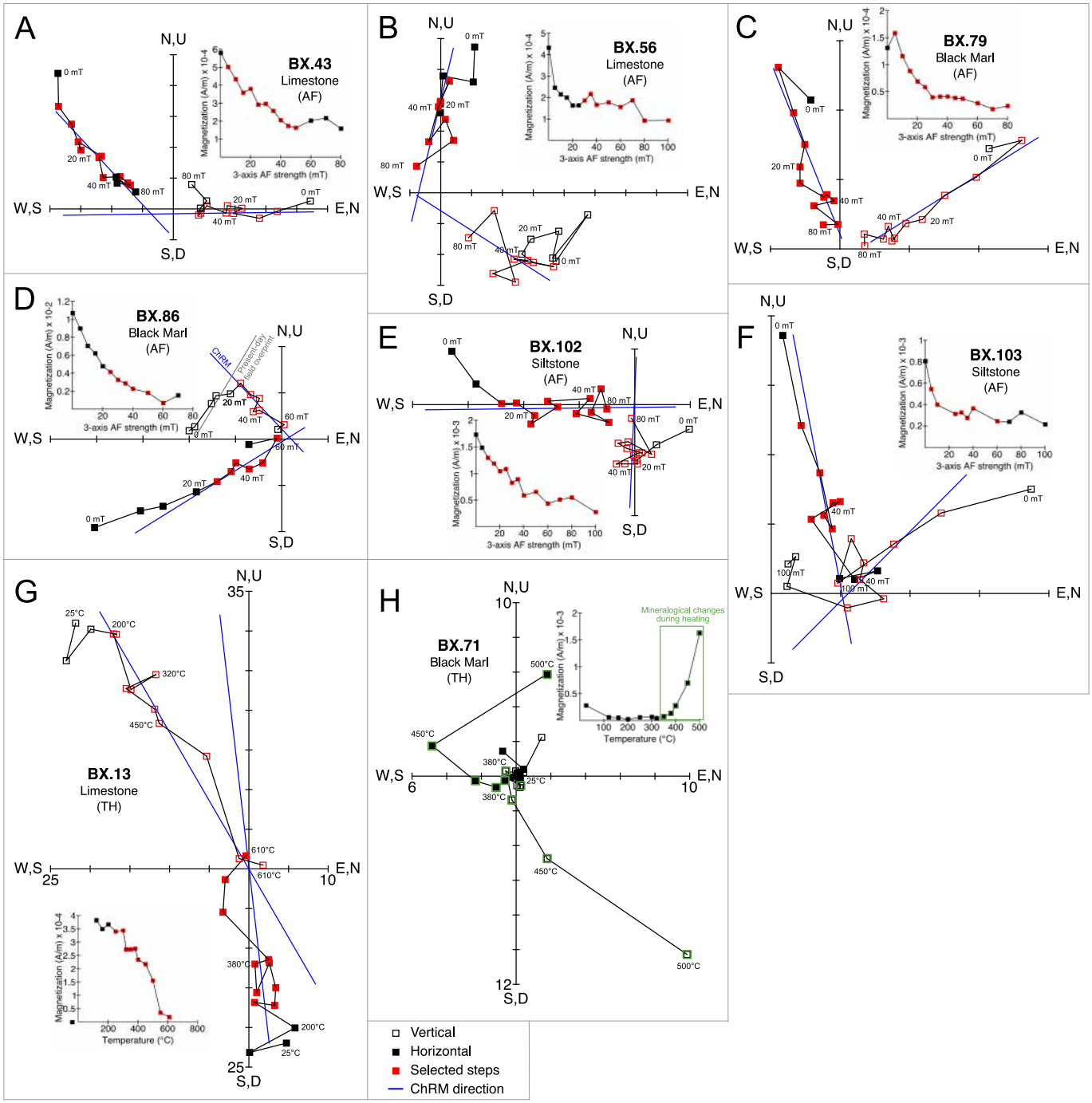

Fig. 3. Zijderveld diagrams and intensity plots for representative samples after Alternalting field (AF) and Thermal (TH) demagnetization.

the medium ranges of demagnetizations coercivities and temperatures and with the absence of macroscopic alteration phases in the samples suggests that the ChRM is relative to primary magnetization and potentially carried by magnetite or titano-magnetite.

4.2. Biostratigraphy of Çamili Mezra and Ciçekdagi

Samples from the Çamili Mezra section yield 15 genera and 37 species of planktonic foraminifera, which are attributed to two different zones. Samples AR22-BiO1 and BiO2 are attributed to the *Globigerinatheka kugleri/Morozovella aragonensis* Concurrent- range Zone (E9 Zone of Berggren and Pearson (2005)). Sample ARR22-BiO3 and BiO4, which are higher in the section, are attributed to the *Acarinina topilensis* Partial-range Zone (E10 Zone of Berggren and Pearson (2005)). The Geological Time Scale indicates a middle Lutetian age for both zones, ca. 44.0–43.3 Ma for E9 and ca. 43.3–42.0 Ma for E10 (Speijer et al., 2020). Sample CIC22-BiO1 from the Ciçekdagi mine yields 8 genera and 16 species from planktonic foraminifera and 8 genera and 8 species from ostracods which indicate an affinity with the *Guembelitrioides nuttalli* Lowest-occurence Zone (E8 Zone of Berggren and Pearson (2005)). The E8 zone is early Lutetian, ca. 46.2–44.0 Ma (Speijer et al., 2020).

4.3. Geochronology of Çamili Mezra, Ciçekdagi and Bultu-Zile

4.3.1. U-Pb dating

Individual $^{238}U/^{206}Pb$ zircon ages and averaged values are displayed on Fig. 4. Concordia plots are also available in Supplementary Information 3. The tuff sample from Bultu-Zile mine site BZ1 yields an early Lutetian 45.1 ± 0.9 Ma (2σ) age. Mine site BZ2 yields a slightly older 46.5 ± 1.0 Ma (2σ) age, but the 95 % confidence interval of both ages overlap. Detrital zircons from sample AR22DZ2, at the base of the Çamili Mezra site, yields an Ypresian maximum depositional age of 50.6 ± 2.9 Ma (2σ; based on the 3 youngest zircons). Detrital zircons from sample 23CMXDZ, at the base of the Ciçekdagi mine, yields an older, Paleocene maximum depositional age of 61.6 ± 1.1 Ma (2σ; based on the 3 youngest zircons).

4.3.2. ^{40}Ar-^{39}Ar dating

The shape of the age spectrum provided by the $^{40}Ar/^{39}Ar$ degassing experiment shows a decrease in apparent ages from ca. 48.5 Ma in the low temperature steps down to ca. 43.5 Ma for the fusion step (Fig. 5A). This may evoke disturbances related to $^{39}Ar_K$ recoil during neutron irradiation (Turner and Cadogan, 1974; Harrison, 1983; Ruffet et al., 1991; Foland et al., 1992), with a possible recoil induced $^{39}Ar_K$ redistribution. However, in support of this scenario, the first steps of degassing lack a $^{39}Ar_K$ discharge decoupled from the degassing of a radiogenic component ($^{40}Ar^*$), since it has been displaced by the recoil phenomenon and is poorly trapped in a crystal lattice.

On the other hand, the shape of this age spectrum can be interpreted differently if we consider the mineralogical heterogeneity of the analysed material, a millimetre-sized fragment of whole rock, and the degassing kinetics during the $^{40}Ar/^{39}Ar$ experiment. The $^{37}Ar_{Ca}/^{39}Ar_K$ spectrum shows that more potassic or less calcic phases are expressed in the first part of the degassing of the sample than those that tend to be expressed at higher temperatures (Fig. 5A). Degassing of these more potassic phases is predominant, as indicated by the main peak in the $^{39}Ar_K$ degassing spectrum $[(^{39}Ar_K/\Delta V_{T^\circ})/(^{39}Ar_K/\Delta V_{T^\circ})_{Max}$ versus $\%^{39}Ar_K$ (de Putter and Ruffet, 2020; Tremblay et al., 2020) and its expression via the weighted age spectrum [Apparent ages versus $(^{39}Ar_K/\Delta V_{T^\circ})/(^{39}Ar_K/\Delta V_{T^\circ})_{Max}$ versus $\%^{39}Ar_K$] which incorporates degassing kinetics (Fig. 5A). The pseudo-plateau age of 46.6 ± 0.2 Ma (1 s) calculated from the apparent age segment of the age spectrum could be the age of the radiogenic component hosted by these more potassic phases and could be the age of basalt emplacement or contemporaneous

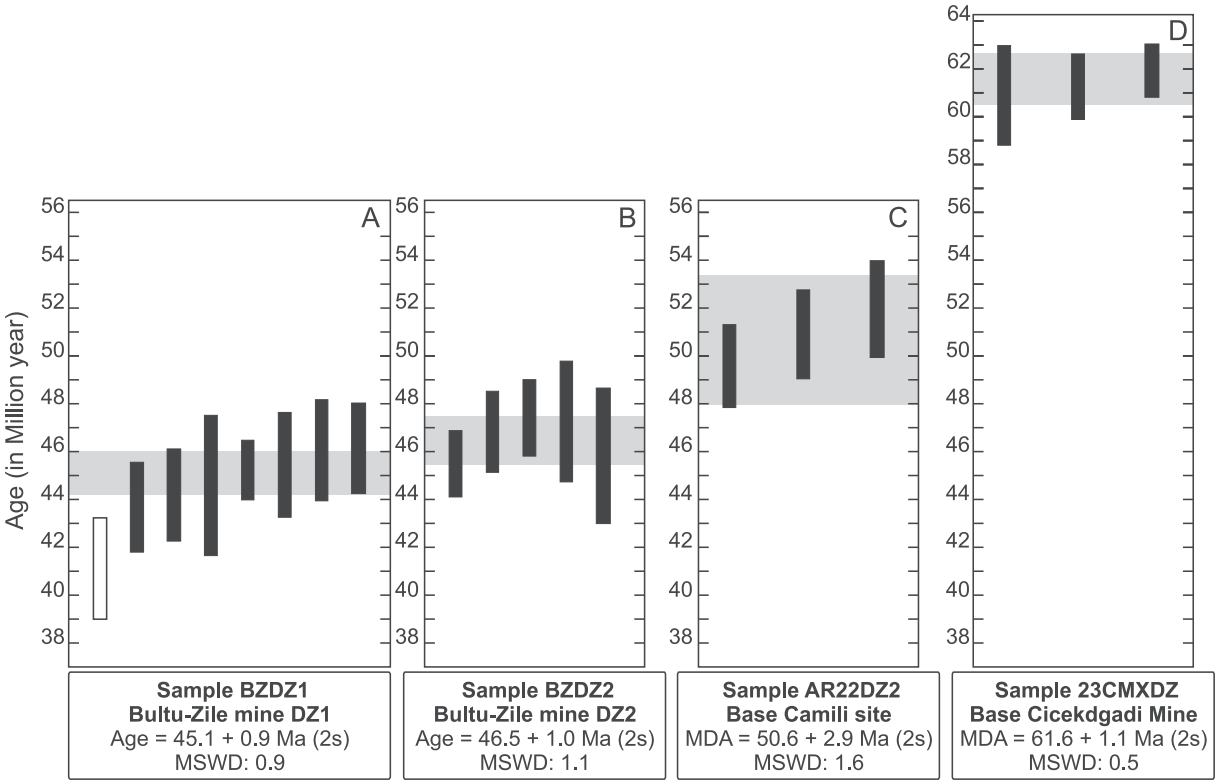

Fig. 4. Individual concordant zircon dates and crystallization ages for samples BZZ1 (A: Bultu-Zile Mine site BZ1) and BZZ2 (B: Bultu-Zile Mine site BZ2), and youngest zircons and related maximum depositional ages (MDA) for samples AR22DZ2 (C: below the Çamili Mezra site) and 23CMXDZ (D: below the Ciçekdagi mine). Black bars: zircon ages used for the age calculation (2σ); white bars: rejected zircon ages (2σ). Grey shades: 95% confidence level for the calculated ages. Final ages include the systematic analytical error. MSWD: Mean Square Weighted Deviation. Calculations and diagrams made with TuffZirc (Ludwig, 2003).

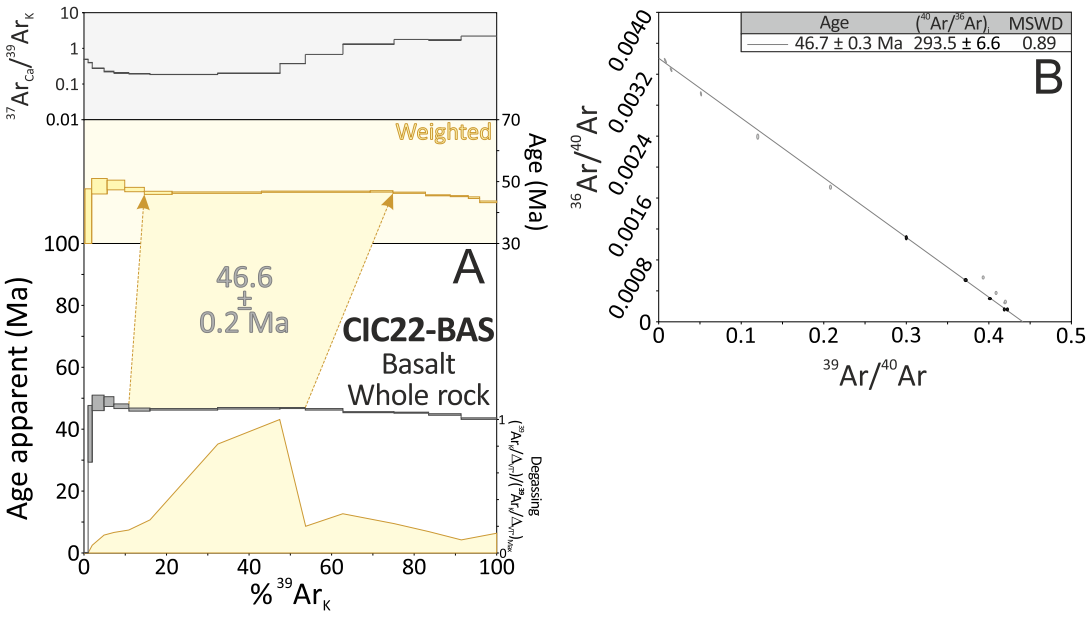

Fig. 5. $^{40}Ar/^{39}Ar$ age and $^{37}Ar_{Ca}/^{39}Ar_K$ (# Ca/K with $^{37}Ar_{Ca}/^{39}Ar_K = CaO/K_2O$ / 2.179); Deckart et al. (1997)) and degassing $((^{39}Ar_K/\Delta V_{T^\circ})/(^{39}Ar_K/\Delta V_{T^\circ})_{Max}$ versus $\%^{39}Ar_K$) and weighted age (see De Putter & Ruffet (2020) and Tremblay et al. (2020) for explanation) spectra and inverse isochron ($^{36}Ar/^{40}Ar$ vs. $^{39}Ar/^{40}Ar$) diagrams of whole rock single grain of basalt CIC22-BAS. Apparent age error bars are at the 1σ level; errors in the J-parameter are not included. Pseudo-plateau and isochron ages are given with 1σ uncertainties and include errors in the J-parameter. Grey ellipses are excluded from isochron regression, MSWD stands for Mean Squares of Weighted Deviates.

alteration. This age is validated by the processing in the inverse isochron diagram (correlation diagram) ($^{36}Ar/^{40}Ar$ vs. $^{39}Ar_K/^{40}Ar^*$; (Roddick, 1983; Hanes et al., 1985; Ruffet et al., 1997) with an initial ratio $(^{40}Ar/^{36}Ar)_i$ indistinguishable from the atmospheric ratio ($^{40}Ar/^{36}Ar$ = 298.56 according to Lee et al. (2003) and an MSWD in accordance with statistical validity criteria (Fig. 5B). The decrease in apparent ages associated with the degassing of the calcic phases at high temperatures could reflect the effects of later weathering of the basalt, which was more prone to affect its calcic components.

5. Discussion and Conclusion

5.1. Age of the fossil localities

The paleomagnetic polarity sequence of the Çamili Mezra section is determined from the reversal angle of the ChRM directions (Fig. 6, SI Table 1). Two normal (N1, N2) and two reverse (R1, R2) magnetozones are recognized and correlated with the Geomagnetic Time Scale (Speijer et al., 2020).

The preferred scenario correlates the normal magnetozone N2 with the Chron C20n (42.2–43.5 Ma), the reverse magnetozone R1 with the Chron C19r (41.2–42.2 Ma) and the normal magnetozone N1 with the Chron 19n (41.0–41.2 Ma; Fig. 6). The reverse magnetozone R2, which includes the fossil site and detrital zircon sample AR22DZ2, is correlated with the Chron C20r (43.5–46.2 Ma). The base of the section shows normal polarities, and alternative correlations could interpret them as part of the Ypresian sub-magnetozones (C24 to C21, ~54 to 46 Ma), consistent with the late Ypresian age (SBZ11–12, ~51 to 48 Ma) proposed by Schweitzer et al. (2007) for the Kocaçay Formation. However, this interpretation is unlikely for two reasons: (1) these normal polarities are isolated and derived from siltstone samples showing noisy demagnetization diagrams, and (2) it does not align with the late Lutetian age (from biozone E10 to E9, ~44 to 42 Ma) indicated by planktonic foraminiferal biostratigraphy of samples AR22-BiO1 to −BiO4 collected from the Cevirme and Kocaçay Formations (Fig. 6). Moreover, it is inconsistent with the Lutetian age suggested by pollen assemblages from Çamili Mezra for the Cevirme Formation (Akgün et al., 2002) and with the Lutetian age indicated by foraminiferal assemblages from other parts of the basin for the Kocaçay Formation (Nairn et al., 2013).

The preferred correlation indicates a time-lag of 5 to 8 Ma between the deposition age of sample AR22DZ2 and its detrital zircon age, which is common in areas away from subduction margins (Jian et al., 2022). Sedimentation rates ranging from 3.3 to 3.8 cm/ka are estimated (SI Table 3) for the marly Cevirme Formation and the limestone-dominated Kocaçay Formation indicating near constant siliciclastic input during basin depth shallowing. This correlation confirms the Lutetian age for the entirety of the Çamili Mezra section, now spanning from 46.2 Ma to 41.0 Ma (C20r to C19n). The fossil horizon, located at the top of the Barakle Fm falls within the Chron C20r yielding an age spanning from 46.2 Ma to 43.5 Ma. Using a mean accumulation rate of 3.5 cm/ka and the depth of the fossil horizon (e.g. 46 m below the R2-N2 transition attributed to the C20n-C20r reversal, dated at 43.5 Ma in Speijer et al. (2020)), we estimate an age of ~ 45 Ma for the fossil horizon (SI Table 3).

In Ciçekdagi, our biostratigraphy sample (CIC22-BiO1) yields an early Lutetian age for the fossiliferous lignite material (planktonic foraminiferal biozone E8: 46.2–44.0 Ma), which is compatible with the Lutetian age indicated by the pollen assemblage of the lignite bed (Akgün, 2002). ^{40}Ar-^{39}Ar dating of a basaltic dyke yields a pseudo-plateau age of 46.6 ± 0.4 Ma (2 s), providing a minimum age for the fossil locality. This age is compatible with our biostratigraphic age only if the fossil bed lies at the very base of biozone E8 (e.g. at ca. 46.2 Ma). We note that the age of the base of biozone E8 is aligned with the base of Chron C20r in the Geological time scale (Speijer et al., 2020). We thus attribute the Ciçekdagi fossil bed to the very base of Chron C20r (ca. 46.2 Ma). This age is compatible with the Paleocene maximum depositional age based on the detrital zircon of sample 23CMXDZ, just below the lignite bed.

The Ciçekdagi and Çamili Mezra fossil sites are thus attributed to the same Chron (C20r). While Ciçekdagi is dated to the very base of the chron, Çamili Mezra is likely slightly younger within the chron (ca. 1.2 Ma younger based on accumulation rate estimates). We note that both lignite beds reflect the continental-to-marine transition in a regional, Lutetian marine transgression. The diachronicity between both sites can

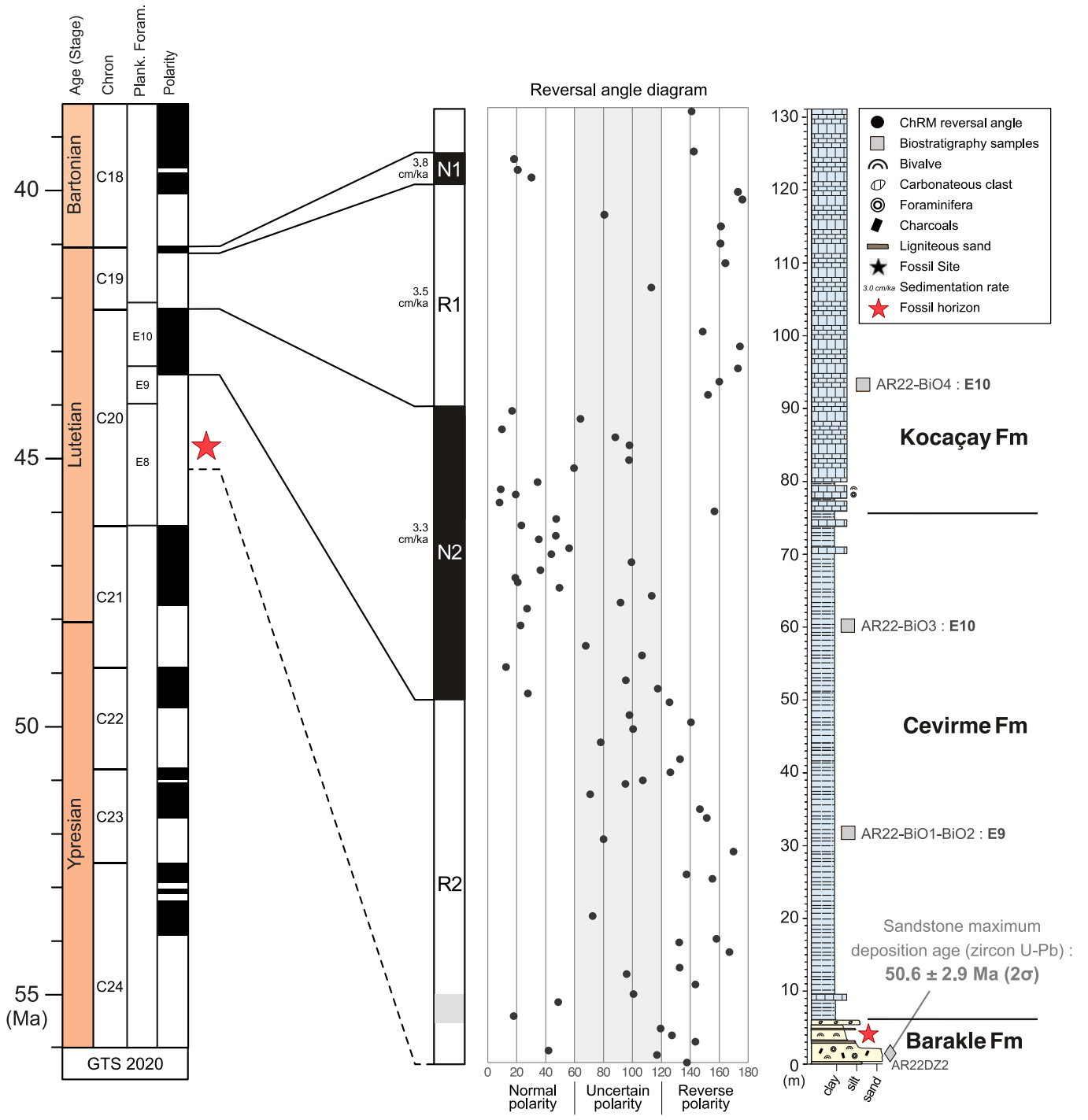

Fig. 6. Stratigraphic log of Çamili Mezra, reversal angle diagram (estimated from an expected direction of D = 0° and I = 50°), associated magnetozones interpretation (N1, N2, R1, R2) and magnetostratigraphic correlation with the Paleogene Geomagnetic Polarity Time Scale (Speijer et al., 2020). The fossil horizon age was estimated according to its position in the section and section-mean an accumulation rate of 3.5 cm/ka.

thus be explained by the fact that Ciçekdagi is ca. 10 km basinward compared to Çamili Mezra: the transition to marine conditions is thus expected to occur first in Ciçekdagi and later in Çamili Mezra.

U-Pb dating of two tuff samples in Bultu-Zile (BZZ1: 45.1 ± 0.9 Ma; BZZ2: 46.5 ± 1.0 Ma; 2 s) indicate an early Lutetian age for both localities. It is unclear if the two Bultu-Zile mines represent the same lignite horizon or two distinct horizons yielding similar fossil material. Nonetheless, both ages overlap over the 45.5–46.0 Ma time window which could support a similar age for both mines. These ages overlap with the age of Ciçekdagi and Çamili Mezra localities.

5.2. *Constraining the chronology of Balkanatolian endemism*

The age range for the Ciçekdagi and Bultu-Zile localities was precedently defined as Ypresian to Lutetian (Licht et al., 2022) while the Camili Mezra locality was attributed to the Ypresian (Métais et al., 2024). This study refines the age of these three localities and indicates tight and coherent ages spanning the early Lutetian (ca. 47.5 Ma to 43.5 Ma).

Overall, fossil sites yielding endemic Balkanatolian mammals are dominantly Lutetian (Fig. 7). The only site unequivocally attributed to

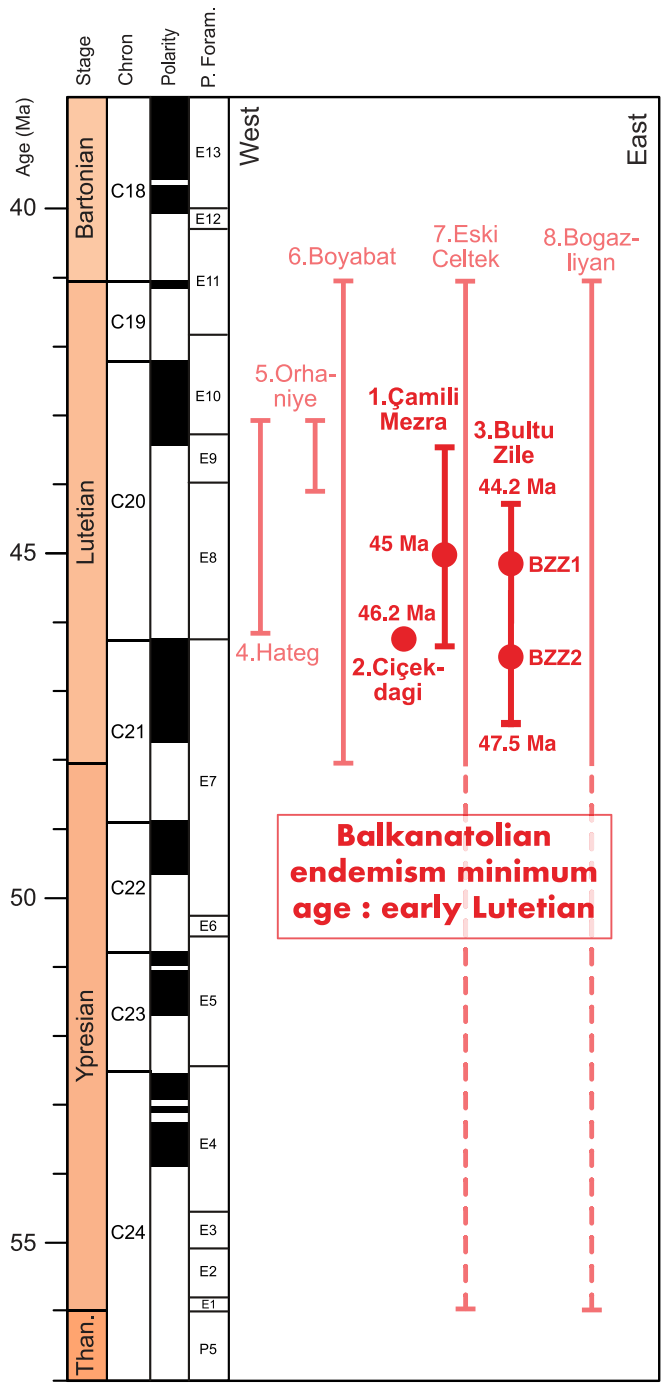

Fig. 7. Age uncertainty of individual Balkanatolian-derived fossil localities sorted from west to east, modified from Licht et al. (2020). In bold: new ages from this study. Dots: Estimated ages and their uncertainty; Cicekdagi: 46.2 Ma; Camili Mezra: 45 Ma; Bultu-Zile (BZZ1): 45.1 ± 0.9 Ma (2 s); Bultu-Zile (BZZ2): 46.5 ± 1.0 Ma (2 s).

times older than Lutetian is the Eski Celtek coal mine site, yielding the embrithopod *P. kansui* as well as the pleuraspidotheriid *Parabunodon anatolicum* (Métais et al., 2012). Indeed, planktonic foraminifera of Ypresian age have been found above the Eski Celtek lignite member (Koç and Türkmen, 2002). We note however that the pollen assemblage of the Eski Celtek lignite indicates a Lutetian age (Akgün et al., 2002), and that this biostratigraphic incompatibility recalls the one previously found at Camili Mezra, where the Lutetian age indicated by pollen ends up to be the most compatible with our magnetostratigraphic and biostratigraphic constraints. We thus consider a Lutetian age for the Eski Celtek lignite as likely as the proposed Ypresian age, pending further work on the locality. The only other putative Ypresian site is the Bogazlıyan-Yeni Fakili locality, also yielding the embrithopod *P. kansui*, age uncertainty spanning over the Ypresian and Lutetian (Sen and Heintz, 1979) (Fig. 7). The exact location of this site has been lost, and our efforts in the field to locate this site have been so far vain, impeding the acquisition of tighter age constraints. There is therefore, so far, no unequivocally-dated Cenozoic fossil locality with terrestrial vertebrate remains on Balkanatolia before the early Lutetian.

Pending further dating of the Eski Celtek and Bogazlıyan-Yeni Fakili localities, our new ages thus provide an early Lutetian minimum age for the first uniquely embrithopod-bearing site on the northern shores of the Neotethys. Although there are no unequivocally-dated Cenozoic fossil localities with terrestrial vertebrates on Balkanatolia before the early Lutetian, there are compelling reasons to infer that the actual onset of endemism occurred prior to the Lutetian. The persistence of pleuraspidotheriids in Balkanatolia (which went extinct before the end of Paleocene elsewhere), as well as the absence of clades that became ubiquitous across Laurasia during the earliest Eocene (such as rodents, perissodactyls, artiodactyls, and carnivorans), suggest a biogeographic isolation since at least the latest Paleocene (Métais et al., 2018; Licht et al., 2017). We are thus still missing the earliest part of Balkanatolian endemism history. Consequently, questions such as how and when embrithopods and other invasive clades reached Balkanatolia remain open, calling for further prospection and identification of earlier fossil sites.

The oldest embrithopod remains outside Balkanatolia are so far dated to the middle Ypresian in Morocco (Gheerbrant et al., 2021) which supports an African origin for the clade (Sen, 2013). The early Lutetian age of our localities provides a minimum age for the overwater dispersal of embrithopod out of Africa. They also show the synchronous presence of at least two genera of embrithopods as early as the early Lutetian, *Crivadiatherium* and *Paleoamasia*, supporting an early diversification of the clade soon after they reached Balkanatolian shores (Métais et al., 2024).

CRediT authorship contribution statement

Leny Montheil: Writing – review & editing, Writing – original draft, Visualization, Investigation, Formal analysis, Data curation, Conceptualization. **Alexis Licht:** Writing – review & editing, Writing – original draft, Visualization, Validation, Supervision, Resources, Project administration, Methodology, Investigation, Funding acquisition, Formal analysis, Data curation, Conceptualization. **Deniz İbilioğlu:** Writing – review & editing, Writing – original draft, Formal analysis, Data curation. **Paul Botté:** Writing – review & editing, Formal analysis, Data curation. **Faruk Ocakoğlu:** Writing – review & editing, Investigation. **François Demory:** Writing – review & editing, Methodology. **Gilles Ruffet:** Writing – original draft, Formal analysis, Data curation. **Abel Guihou:** Writing – review & editing, Methodology, Formal analysis. **Mustafa Kaya:** Writing – review & editing, Investigation. **Benjamin Raynaud:** Writing – review & editing, Investigation. **Mehmet Serkan Akkiraz:** Writing – review & editing, Investigation. **Pierre Deschamps:** Writing – review & editing, Methodology. **Grégoire Métais:** Writing – review & editing, Investigation. **Pauline Coster:** Writing – review & editing, Investigation. **K. Christopher Beard:** Writing – review & editing, Investigation, Funding acquisition.

Declaration of competing interest

The authors declare that they have no known competing financial interests or personal relationships that could have appeared to influence the work reported in this paper.

Acknowledgments

This work was supported by grants from the U.S. National Science Foundation (EAR-1543684 and EAR-2141115) to KCB, National Geographic Society CRE GRANT #9215-12 to GM, and the European Research Council (ERC) under the European Union's Horizon 2020 research and innovation program (grant agreement No. 101043268) to AL. We thank Davut Şahin, Julien Longerey, and Josué Dauvier for prolific discussions and assistance in the field and in the lab. This article is dedicated to the memory of Çelik Ocakoğlu, who participated in many of our field trips.

Appendix A. Supplementary material

Supplementary data to this article can be found online at https://doi.org/10.1016/j.jseaes.2025.106661.

Data availability

Data will be made available on request.

References

Akkiraz, M.S., Kayseri, M.S., Akgün, F., 2008. Palaeoecology of coal-bearing Eocene sediments in Central Anatolia (Türkiye) based on quantitative palynological data. Turk. J. Earth Sci. 17, 317–360.

Akgün, F., 2002. Stratigraphic and paleoenvironmental significance of eocene palynomorphs of the corum-amasya area in the central anatolia, Türkiye. Acta Palaeontol. Sin. 41, 576–591.

Akgün, F., Akay, E., Erdogan, B., 2002. Tertiary terrestrial to shallow marine deposition in Central Anatolia: a palynological approach. Turk. J. Earth Sci. 11, 127–160.

Barrier, E., Vrielynck, B., Brouillet, et al., 2018. Paleotectonic reconstruction of the central tethyan realm. tectono-sedimentary-palinspastic maps from late Permian to Pliocene. *CCGM/CGMW*, Paris, Atlas of 20.

Beard, K.C., Métais, G., Ocakoğlu, F., et al., 2021. An omomyid primate from the Pontide microcontinent of north-central Anatolia: implications for sweepstakes dispersal of terrestrial mammals during the Eocene. Geobios 66, 143–152.

Beard, K.C., Coster, P.M., Ocakoğlu, F., et al., 2023. Dental anatomy, phylogenetic relationships and paleoecology of Orhaniyeia nauta (Metatheria, Anatoliadelphyidae), a Gondwanan component of the insular Eocene mammal fauna of Balkanatolia (north-central Türkiye). J. Mamm. Evol. 30, 859–872.

Berggren, W.A., Pearson, P.N., 2005. A revised tropical to subtropical Paleogene planktonic foraminiferal zonation. J. Foraminiferal Res. 35, 279–298.

Cheilletz, A., Ruffet, G., Marignac, C., et al., 1999. 40Ar/39Ar dating of shear zones in the Variscan basement of Greater Kabylia (Algeria). Evidence of an Eo-Alpine event at 128 Ma (Hauterivian–Barremian boundary): geodynamic consequences. Tectonophysics 306, 97–116.

Deckart, K., Feraud, G., Bertrand, H., 1997. Age of Jurassic continental tholeiites of French Guyana/Suriname and Guinea: implications to the opening of the Central Atlantic Ocean. Earth Planet. Sci. Lett. 150, 205–220.

De Putter, T., Ruffet, G., 2020. Supergene manganese ore records 75 Myr-long Campanian to Pleistocene geodynamic evolution and weathering history of the Central African Great Lakes region - Tectonic drives, climate assists. Gondw. Res. 83, 96–117.

Dickinson, W.R., Gehrels, G.E., 2009. Use of U–Pb ages of detrital zircons to infer maximum depositional ages of strata: a test against a Colorado Plateau Mesozoic database. Earth Planet. Sci. Lett. 288, 115–125.

Erdal, O., Antoine, P.O., Sen, S., 2016. New material of P alaeoamasia kansui (Embrithopoda, Mammalia) from the Eocene of Türkiye and a phylogenetic analysis of Embrithopoda at the species level. Palaeontology 59, 631–655.

Foland, K.A., Hubacher, F.A., Arehart, G.B., 1992. $^{40}Ar/^{39}Ar$ dating of very fined grained samples: an encapsulated-vial procedure to overcome the problem of ^{39}Ar recoil loss. Chem. Geol. 102, 269–276.

Gheerbrant, E., Khaldoune, F., Schmitt, A., Tabuce, R., 2021. Earliest Embrithopod Mammals (Afrotheria, Tethytheria) from the Early Eocene of Morocco: anatomy, systematics and phylogenetic significance. J. Mamm. Evol. 28, 245–283.

Gülyüz, E., Kaymakci, N., Meijers, M.J., et al., 2013. Late Eocene evolution of the Çiçekdagi Basin (central Türkiye): Syn-sedimentary compression during microcontinent–continent collision in central Anatolia. Tectonophysics 602, 286–299.

Hanes, J.A., York, D., Hall, C.M., 1985. An 40Ar/39Ar geochronological and electron microprobe investigation of an Archean pyroxenite and its bearing on ancient atmospheric compositions. Can. J. Earth Sci. 22, 947–958.

Harrison, T.M., 1983. Some observations on the interpretation of $^{40}Ar/^{39}Ar$ age spectra. Chem. Geol. 1, 319–338.

Jian, D., Williams, S.E., Yu, S., et al., 2022. Quantifying the link between the detrital zircon record and tectonic settings. J. Geophys. Res. Solid Earth 127, e2022JB024606.

Jones, M.F., Coster, P.M., Licht, A., et al., 2019. A stem bat (Chiroptera: Palaeochiropterygidae) from the late middle Eocene of northern Anatolia: implications for the dispersal and palaeobiology of early bats. Palaeobiodivers. Palaeoenviron. 99, 261–269.

Jourdan, F., Verati, C., Féraud, G., 2006. Intercalibration of the Hb3gr $^{40}Ar/^{39}Ar$ dating standard. Chem. Geol. 231, 177–189.

Kaya, T., 1995. Palaeoamasia kansui (mammalia) in the Eocene of Bultu-Zile (Tokat-Northeastern Türkiye) and systematic revision of Palaeomasia. Turk. J. Earth Sci. 4, 105–111.

Kirschvink, J.L., 1980. The least-squares line and plane and the analysis of palaeomagnetic data. Geophys. J. Int. 62, 699–718.

Koç, C., Türkmen, I., 2002. Sedimentological characteristics of the coal-bearing Eocene deposits at the north of Suluova (Amasya). Bull. Earth Sci. Appl. Res. 26, 101–117.

Köhler, M., Moyà-Solà, S., 2004. Reduction of brain and sense organs in the fossil insular bovid Myotragus. Brain Behav. Evol. 63, 125–140.

Licht, A., Coster, P., Ocakoğlu, F., et al., 2017. Tectono-stratigraphy of the Orhaniye Basin, Türkiye: Implications for collision chronology and Paleogene biogeography of central Anatolia. J. Asian Earth Sci. 143, 45–58.

Licht, A., Métais, G., Coster, P., et al., 2022. Balkanatolia: The insular mammalian biogeographic province that partly paved the way to the Grande Coupure. Earth Sci. Rev. 226, 103929.

Licht, A., Coster, P., Botté, P., et al., 2024. Sedimentology and chronostratigraphy of the Apt Basin, Southeastern France: lacustrine response to late Paleogene cooling and regional rifting. Bull. De La Société Géologique De France 195, 22.

Ludwig, K. R., 2003. User's manual for IsoPlot 3.0. A geochronological toolkit for Microsoft Excel, 71.

Lurcock, P.C., Wilson, G.S., 2012. PuffinPlot: a versatile, user-friendly program for paleomagnetic analysis. Geochem. Geophys., Geosyst. 13.

Maas, M.C., Thewissen, J.G.M., Kappelman, J., 1998. Hypsamasia seni (Mammalia: Embrithopoda) and other mammals from the Eocene Kartal Formation of Türkiye. Bull. Carnegie Museum Nat. History 34, 286–297.

MacArthur, R.H., Wilson, E.O., 1963. An equilibrium theory of insular zoogeography. Evolution 373–387.

MacArthur, R.H., Wilson, E.O., 1967. The Theory of Island Biogeography. Princeton, Princeton University Press.

Métais, G., Gheerbrant, E., Sen, S., 2012. Re-interpretation of the genus Parabunodon (Ypresian, Türkiye): implications for the evolution and distribution of pleuraspidotheriid mammals. Palaeobiodivers. Palaeoenviron. 92, 477–486.

Métais, G., Albayrak, E., Antoine, P.O., et al., 2016. Oligocene ruminants from the Kızılırmak Formation, Çankırı-Çorum Basin, Central Anatolia. Türkiye. Palaeontologia Electronica 19–113.

Métais, G., Coster, P.M., Kappelman, J.R., et al., 2018. Eocene metatherians from Anatolia illuminate the assembly of an island fauna during Deep Time. PLoS One 13, 11.

Métais, G., Coster, P., Licht, A., et al., 2023. Additions to the late Eocene Sungulu mammal fauna in Easternmost Anatolia and the Eocene-Oligocene transition at the periphery of Balkanatolia. C.R. Palevol 35, 35.

Métais, G., Coster, P., Kaya, M., et al., 2024. Rapid colonization and diversification of a large-bodied mammalian herbivore clade in an insular context: New embrithopods from the Eocene of Balkanatolia. J. Mamm. Evol. 31, 15.

Mueller, M.A., Licht, A., Campbell, C., et al., 2022. Sedimentary provenance from the evolving forearc-to-foreland Central Sakarya Basin, western Anatolia reveals multi-phase intercontinental collision. Geochem. Geophys., Geosyst. 23.

Myers, N., Mittermeier, R.A., Mittermeier, C.G., et al., 2000. Biodiversity hotspots for conservation priorities. Nature 403, 853–858.

Nairn, S.P., Robertson, A.H., Ünlügenç, U.C., et al., 2013. Tectonostratigraphic evolution of the Upper Cretaceous–Cenozoic central Anatolian basins: an integrated study of diachronous ocean basin closure and continental collision. Geol. Soc. Lond. Spec. Publ. 372, 343–384.

Ozansoy, F., 1966. Türkiye senozoik çağlarında fosil insan formu prblemi ve biostratigrafik dayanakları 172. Ankara Üniversitesi Basımevi.

Poblete, F., Dupont-Nivet, G., Licht, A., et al., 2021. Towards interactive global paleogeographic maps, new reconstructions at 60, 40 and 20 Ma. Earth Sci. Rev. 103508.

Popov, S.V., Rögl, F., Rozanov, A.Y., et al., 2004. Lithological-paleogeographic maps of Paratethys-10 maps late Eocene to Pliocene. CFS Courier Forschungsinstitut Senckenberg 250, 1–46.

Proust, J.N., Hosu, A., 1996. Sequence stratigraphy and Paleogene tectonic evolution of the Transylvanian Basin (Romania, eastern Europe). Sed. Geol. 105, 117–140.

Radulesco, C., Samson, P., 1987. Eocene mammals from Romania with a review of embrithopods. The Eocene from the Transylvanian Basin. Universitatea Babes-Bolyai, Cluj-Napoca, Romania, 135-142.

Roddick, J., 1983. High precision intercalibration of ^{40}Ar-^{39}Ar standards. Geochim. Cosmochim. Acta 47, 887–898.

Renne, P.R., Mundil, R., Balco, G., et al., 2010. Joint determination of ^{40}K decay constants and $^{40}Ar^*/^{40}K$ for the Fish Canyon sanidine standard, and improved accuracy for $^{40}Ar/^{39}Ar$ geochronology. Geochim. Cosmochim. Acta 74, 5349–5367.

Renne, P. R., Balco, G., Ludwig, K. R., et al., 2011. Response to the comment by WH Schwarz et al. on "Joint determination of 40K decay constants and 40Ar*/40K for the Fish Canyon sanidine standard, and improved accuracy for 40Ar/39Ar geochronology" by PR Renne et al.(2010). *Geochimica et Cosmochimica Acta*, *75*, 5097-5100.

Ruffet, G., Féraud, G., Amouric, M., 1991. Comparison of ^{40}Ar-^{39}Ar conventional and laser dating of biotites from the North Trégor Batholith. Geochimica Cosmochimica Acta 55, 1675–1688.

Ruffet, G., Gruau, G., Balèvre, M., et al., 1997. Rb-Sr and ^{40}Ar-^{39}Ar laser probe dating of high-pressure phengites from the Sesia zone (Western Alps): underscoring of excess argon and new age constraints on the high-pressure metamorphism. Chem. Geol. 141, 1–18.
Schweitzer, C.E., Shirk, A.M., Ćosović, V., et al., 2007. New species of Harpactocarcinus from the Tethyan Eocene and their paleoecological setting. J. Paleo. 81, 1091–1100.
Sen, S., Heintz, E., 1979. Palaeoamasia kansui Ozansoy 1966, embri– thopode (Mammalia) de l'Eocène d'Anatolie. In Annales De Paléontologie (vértébres) 65, 73–91.
Sen, S., 2013. Dispersal of African mammals in Eurasia during the Cenozoic: ways and whys. Geobios 46, 159–172.
Sevin, M., Uğuz, F.M., Sarıfakıoğlu, E., 2014. 1: 100000 ölçekli Türkiye Jeoloji Haritaları, 205, Çorum–H33 Paftası. Maden Tetkik ve Arama Genel Müdürlüğü, Jeoloji Etütleri Dairesi, Ankara.
Speijer, R.P., Pälike, H., Hollis, et al., 2020. The paleogene period. In: Geologic time scale 2020. Elsevier, pp. 1087–1140.
Steadman, D.W., Martin, P.S., MacPhee, R.D.E., et al., 2005. Asynchronous extinction of late Quaternary sloths on continents and islands. Proc. Natl. Acad. Sci. 102, 11763–11768.
Tremblay, A., Ruffet, G., Lemarchand, J., 2020. Timing and duration of Archean orogenic gold deposits in the Bourlamaque pluton, Val d'Or mining camp, Abitibi Canada. Ore Geol. Rev. 127, 103812.
Turner, G., Huneke, J.C., Podose, F.A., et al., 1971. ^{40}Ar/^{39}Ar ages and cosmic ray exposure ages of Apollo 14 samples. Earth Planet. Sci. Lett. 12, 19–35.
Turner, G., Cadogan, P.H., 1974. Possible effects of ^{39}Ar recoil in ^{40}Ar-^{39}Ar dating. Proceedings of the Fifth Lunar Science Conference 2, 1601–1615.
Uguz, M.F., Sevin, M., Duru, M. 2002. Geological Map of Türkiye, Sinop, 1/500000.
Van der Geer, A., Lyras, G., de Vos, J., et al., 2011. Evolution of Island Mammals: Adaptation and Extinction of Placental Mammals on Islands. John Wiley & Sons.
Van Hinsbergen, D.J., Torsvik, T.H., Schmid, S.M., et al., 2020. Orogenic architecture of the Mediterranean region and kinematic reconstruction of its tectonic evolution since the Triassic. Gondw. Res. 81, 79–229.
Vartanyan, S.L., Garutt, V.E., Sher, A.V., 1993. Holocene dwarf mammoths from Wrangel Island in the Siberian Arctic. Nature 362, 337–340.
Zijderveld, J.D.A., 1967. AC Demagnetization of Rocks: Analysis of Results. In: Runcorn, S.K., Creer, K.M., Collinson, D.W. (Eds.), *Methods in Palaeomagnetism*. Elsevier, pp. 254–286.